Inorganic Nanoparticles Modify the Phase Behavior and Viscoelastic Properties of Non-lamellar Lipid Mesophases

Inorganic Nanoparticles Modify the Phase Behavior and Viscoelastic Properties of Non-lamellar Lipid Mesophases

*Marco Mendozza, Lucrezia Caselli, Costanza Montis, Stefano Orazzini, Emiliano Carretti, Piero Baglioni, Debora Berti**

Department of chemistry Ugo Schiff, University of Florence, and CSGI Via della Lastruccia 3, 50019 Florence, Italy.

*Corresponding Author: debora.berti@unifi.it

ABSTRACT The inclusion of inorganic nanoparticles (NPs) within organized lipid assemblies combines the rich polymorphism of lipid phases with advanced functional properties provided by the NPs, expanding the applicative spectrum of these materials. In spite of the relevance of these hybrid systems, fundamental knowledge on the effects of NPs on the structure and physicochemical properties of lipid mesophases is still limited. This contribution combines Small-Angle X-ray Scattering (SAXS) and Rheology to connect the structural properties with the viscoelastic behavior of liquid crystalline mesophases of Phytantriol (Phyt) containing two kinds of hydrophobic NPs of similar size, i.e., gold NPs (AuNPs) and Superparamagnetic Iron Oxide NPs (SPIONs). Both types of NPs spontaneously embed in the hydrophobic domains of the liquid crystalline mesophase, deeply affecting its phase behavior, as SAXS results disclose. We propose a general model to interpret and predict the structure of cubic mesophases doped with hydrophobic NPs, where the effects on lipid phase behavior depend only on NPs' size and volume fraction but not on chemical identity. The rheological measurements reveal that NPs increase the solid-like behavior of the hybrid and, surprisingly, this effect depends on the chemical nature of the NPs. We interpret these results by suggesting that the long-range dipolar interactions of SPIONs affect the viscoelastic response of the material and provide an additional control parameter on mechanical properties. Overall, this study discloses new fundamental insights into hybrid liquid crystalline mesophases doped with hydrophobic NPs, highly relevant for future applications, e.g. in the biomedical field as smart materials for drug delivery.

KEYWORDS Liquid Crystalline Mesophases; AuNPs; SPIONs; Phytantriol; Cubic Lipid Phases

ABBREVIATIONS LLCs, lyotropic liquid crystals; DDS, drug-delivery systems; Phyt, phytantriol; SPIONs, superparamagnetic iron oxide nanoparticles; AuNPs, gold nanoparticles

1. INTRODUCTION

The inclusion of inorganic nanoparticles into organized lipid assemblies has the potential to combine the properties of the two components to produce smart materials and nanodevices for a variety of diverse applications in the biomedical field. For instance, gold nanorods have been embedded in lipid vesicles for applications in hyperthermia [1,2]; quantum dots-loaded liposomes have been proposed for diagnostic purposes [3–6]; superparamagnetic iron oxide nanoparticles (SPIONs) have been included in liposomes, to form magnetoliposomes, applied both for MRI [7,8] and as drug delivery systems that can release their payload in a space- and time-controlled manner, thanks to responsivity to static and alternating magnetic fields [9–11]. The most explored amphiphilic scaffolds are lipid vesicles, but more recently some studies have addressed the insertion of inorganic NPs [12,13] into non-lamellar lipid assemblies formed through self-assembly of polymorphic lipids. While some applicative examples have been reported, a fundamental understanding of the impact of NPs on lipid phase behavior, necessary to design these materials for a specific biomedical application is, to date, very limited.

It is well known that lipid self-assembly in water gives rise to a rich phase diagram, with a complex variety of architectures and morphologies, as in the case of glyceryl-monooleate (GMO) and Phytantriol (Phyt). For these latter systems, the phase diagrams have been thoroughly investigated over the years [14]. Depending on the water content, lamellar structures (Lc and Lα) and bicontinuous cubic mesophases (gyroid Ia3d and diamond Pn3m) are observed at room temperature, while hexagonal structures and inverted micelles are formed at higher temperatures. The presence of additives modifies and controls the geometry of these lipid architectures. This is the case for fatty acids [15,16], photo-switchable molecules [17–19], and proteins [20] that can be even crystallized within the lyotropic phase [21,22]. Recently, Briscoe et al. [23,24] investigated the effects of hydrophobic silica NPs on dioleoyl-

phopshatidylethanolamine mesophases, highlighting a temperature and pressure-dependent lamellar to hexagonal phase transition. Mezzenga and coauthors studied the inclusion of hydrophilic SPIONs in monolinolein assemblies, observing the structural responsiveness of the lipid-SPION hybrids to static magnetic fields [25,26]. In a previous work, we showed that the addition of hydrophobic SPIONs to a GMO Pn3m cubic phase induces a transition to hexagonal phase, which can be understood as a balance between the free energies of membrane elastic curvature and lipid frustration packing [27]. Additionally, we highlighted that the same phase transition occurs by applying a low frequency alternating magnetic field (AMF), due to the local heating produced by the magnetic relaxation of NPs [27,28].

The central purpose of this study the separation of thermodynamic effects, due to insertion of hydrophobic hard spheres with a given curvature into locally bilayered structures, from functional effects, specifically originating from the chemical nature of the NPs. To this aim, we leverage our previous studies on hybrid lipid cubic mesophases [27,28] to investigate two kinds of hydrophobic NPs and map the phase and flow behavior with SAXS and Rheology. Phytantriol (Phyt), endowed with lyotropic and thermotropic polymorphism, was doped with NPs characterized by the same size and similar hydrophobic coating, but different core, i.e., AuNPs and SPIONs.

The ensemble of results here gathered, besides providing fundamental knowledge on the phase behavior of such hybrid systems, discloses new insights on the interaction between nanomaterials and non-lamellar biomimetic interfaces at the molecular level, fostering the applicative potentials of these smart materials in the biomedical field [29–32]).

2. MATERIALS AND METHODS

2.1. Materials

Fe(III)-acetylacetonate (97%), 1,2-hexadecanediol (90%), oleylamine (70%), oleic acid (90%), diphenylether (99%), denatured ethanol and hexane mixture of isomers employed for the synthesis of hydrophobic SPIONs, were purchased from Sigma Aldrich (St. Louis MO), the same for Gold-(III) tetrachloride (99.995%), tetraoctylammonium bromide (TOAB 98%). Phytantriol (Phyt) was a gift of Royal DSM. The synthesis of AuNPs and SPIONs is reported in the SI.

2.2. Preparation of bulk cubic mesophases

The preparation of bulk cubic phase with or without SPIONs and AuNPs was performed according to the following procedure: 30 mg of Phyt was weighted into 2 mL glass vessels in the absence of (for neat Phyt mesophases) or in the presence of (for NPs-loaded Phyt mesophases) appropriate volume of SPIONs and AuNPs dispersions in hexane. About 1 mL of hexane was used to solubilize mixture and then the solvent was removed under a gentle nitrogen flux. The dry films were left under vacuum overnight, then hydrated with 50 μL Milli-Q water and centrifuged 5 minutes for five cycles at 10100 G, alternating a run with the cap facing upward with another with the cap facing downward for each cycle.

2.3. Small-Angle X-ray Scattering (SAXS)

SAXS measurements were performed on a S3-MICRO SAXS/WAXS instrument (HECUS GmbH, Graz, Austria) which consists of a GeniX microfocus X-ray Sealed Cu Ka source (Xenocs, Grenoble, France) with power 50 W. The source provides a focused X-ray beam with λ=0.1542 nm Cu Kα line [33,34]. The instrument is equipped with two one-dimensional (1D) position sensitive detectors, (HECUS 1D-PSD-50 M system) each detector is 50 mm long (spatial resolution 54 μm/channel, 1024 channels) and covers a q-range of $0.003 < q < 0.6$ Å^{-1} (SAXS) and $1.2 < q < 1.9$ Å^{-1}, (WAXS). The temperature was controlled by means of a Peltier TCCS-3 Hecus. The SAXS curves of bulk cubic phase were recorded at 25, 35 and 50 °C in a solid sample-holder. The hexane dispersions of SPIONs and AuNPs were inserted in a glass

capillary to record SAXS profiles. The NPs dry films were prepared as follows: the NPs dispersion in hexane was placed in a glass capillary and dried under vacuum overnight to remove the solvent. The SAXS profiles were then recorded. The SAXS data analysis is detailed in the SI.

2.4. Rheology

All rheology tests were performed using a Physica-Paar UDS 200 rheometer, equipped with a plate-plate geometry measuring system (diameter of the upper plate 20 mm, measuring gap: 200 μm). The temperature was controlled with a Peltier device. All the oscillatory measurements were performed within the linear viscoelastic range (1 Hz about the amplitude sweep curves). For all the measurements, once the samples were deposed on the surface of the measuring plate, a delay time of 10 mins was set in order to ensure the complete equilibration of the sample; in that way no loading effect was observed for all the investigated samples. In order to minimize the evaporation of water, silicone oil was applied to the rim of the samples when temperature was varied in 25-50 °C. The instrumental setups for the rheology tests are the following:

i- Frequency sweep test: frequency range 100 Hz to 0.001 Hz; amplitude 0.1% strain;

ii- Amplitude sweep test: strain % from 0.001% to 10%; frequency 1 Hz.

3. RESULTS AND DISCUSSION

3.1 Structure of Phyt mesophases doped with hydrophobic NPs

Figure 1 summarizes the physicochemical characterization of the NPs (AuNPs and SPIONs) employed in the study. Briefly, AuNPs with a dodecanethiol coating in hexane were synthesized according to Brust et al. [35] (see Materials and Methods for details), leading to slightly polydisperse nanospheres, as visible from the TEM images (Figure 1d). The analysis of the NPs' SAXS profile yielded an average core diameter of 3.0 nm and a polydispersity

index of 0.28, as estimated through a Schultz distribution [36] (see Figure 1c): a similar value was obtained from TEM (average diameter 2.8 nm, See SI for details). Hydrophobic SPIONs were synthesized according to Wang et al. [37], leading to a stable hexane dispersion of magnetite nanospheres coated with oleic acid/oleylamine, with slightly larger size than AuNPs, as visible from TEM images (Figure 1b) and from the SAXS (Figure 1a) curve fitting results: core diameter of 3.6 nm (3.8 nm by TEM) and polydispersity of 0.30. The two different NPs' samples are therefore characterized by a hydrophobic coating, which is expected to drive their inclusion in the hydrophobic domains of the mesophase, and by relatively small core size, which is a necessary prerequisite to determine a minimum local perturbation to the bilayered arrangement of Phyt, of 2.8 nm thickness [38].

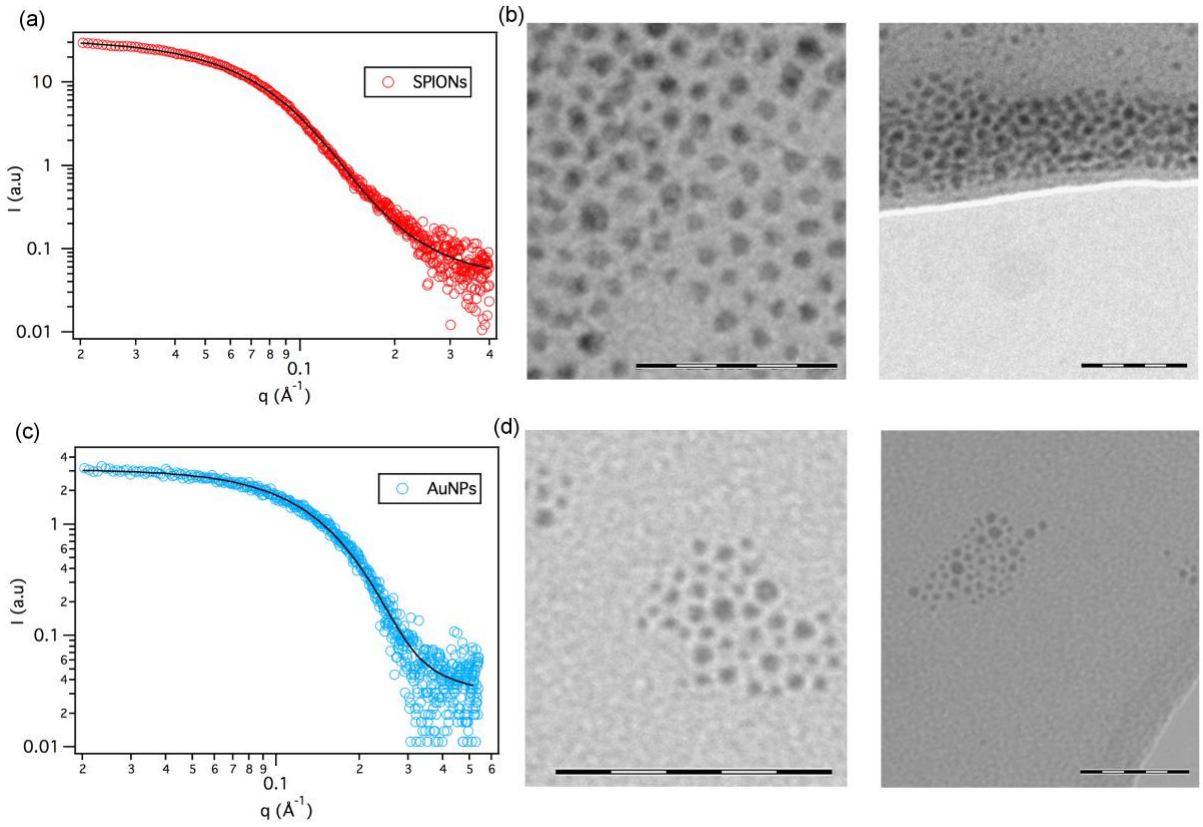

Figure 1. Structural characterization of hydrophobic AuNPs and SPIONs: (a, c) Small-Angle X-ray Scattering profiles of SPIONs (a) and AuNPs (c) in hexane: the continuous lines represent the best fitting curves according to a Schultz polydisperse spheres distribution; (b, d) representative TEM images of (b) SPIONs and (d) AuNPs. The scale bar in TEM image is 50 nm.

The effects of increasing amounts of hydrophobic NPs (SPIONs and AuNPs) on the structure of the liquid crystalline mesophases of Phyt in water excess at 25 °C were then monitored with SAXS (Figure 2a, 2b).

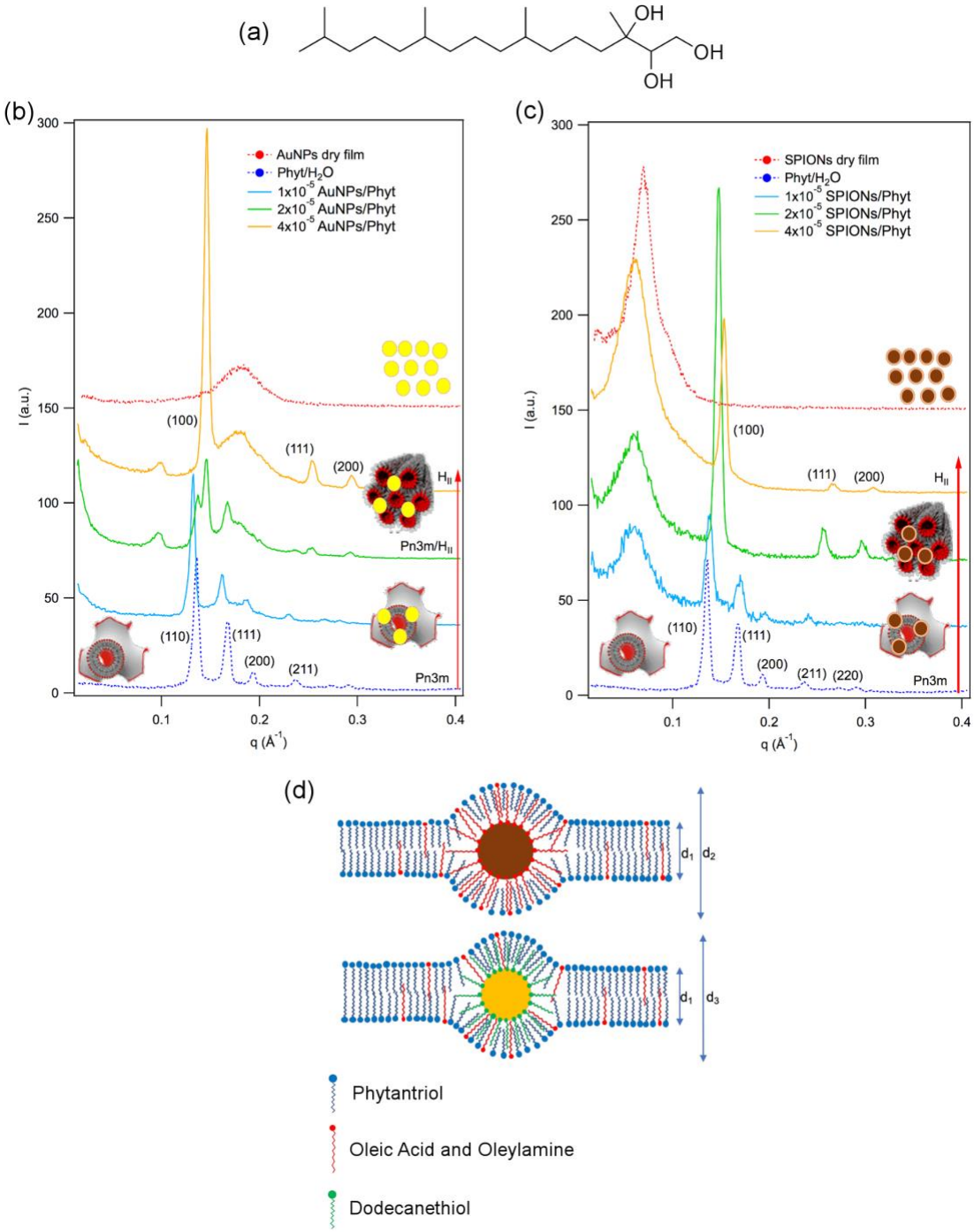

Figure 2. SAXS of Phyt/H_2O mesophases as the concentration ($1x10^{-5}$, $2x10^{-5}$, $4x10^{-5}$ per Phyt molecule) of (b) AuNPs and (c) SPIONs increases, compared to the SAXS profile of Phyt/H_2O in the absence of NPs (blue dashed line) and with the spectra measured for a dry film of (b) AuNPs and (c) SPIONs (dashed red lines); the Miller indexes assignments (hkl) of the Pn3m and hexagonal phase are reported in the graphs. In (d) is reported the nano-scale visualization of NPs encapsulated into the

bilayer. The blue amphiphiles sketch represent phytantriol molecules, red amphiphiles the oleic acid and oleylamine molecules and the green ones dodecanethiol molecules.

It is well known that the binary system Phyt/H_2O with excess water at room temperature is a Pn3m cubic mesophase, with the amphiphilic Phyt molecules assembled as bilayers folded in a tridimensional cubic structure [39]. Accordingly, the Bragg peaks of the cubic phase are clearly recognizable in the corresponding SAXS profile (Figure 2b, 2c, blue dashed lines).

Before discussing the phase behavior of hybrid NPs/Phyt systems, some consideration should be made about the Phyt bilayer thickness as compared with NPs' size. While the former is 2.8 nm[40], the overall sizes of magnetic and gold nanoparticles, considering their shell composed by oleic acid (chain length 2 nm [41]) and dodecanethiol (1.4 nm [42]), are 7.6 nm and 5.8 nm respectively. In the hypothesis of interdigitation between Phyt and the coating alkyl chains, it is mainly the hynderence of NPs' cores to determine a local perturbation in the bilayer (See the sketch in Figure 2d). Dodecanethiol is covalently bound to the surface of AuNPs (the excess is removed during the synthesis work-up, See SI for details), while oleic acid and oleylamine are in excess in SPIONs dispersion. Therefore, to better compare Phyt/SPIONs and Phyt/AuNPs data without coating effects, Phyt/AuNPs samples were prepared adding the same quantity of SPIONs stabilizing agent (See sections S-4 and S-5 in SI for details).

The addition of increasing amounts of both SPIONs and AuNPs (see Materials and Methods for details) results in a clear modification of the mesostructure. Even small amounts of NPs ($1x10^{-5}$ NPs/Phyt) causes the appearance of an additional peak, broad and centered at 0.18 $Å^{-1}$ for AuNPs and more intense and centered at 0.06 $Å^{-1}$ for SPIONs.. These peaks are present for all the Phyt/NPs SAXS profiles (see Figure 2b, 2c), without any significant shift of the maximum, irrespectively of the amounts of NPs. To gain more insight on this effect, we measured the SAXS profiles of dry NPs films (see Materials and Methods for details on samples preparation). The dry AuNPs film (Figure 2b, red curve) exhibits a broad peak, centered at 0.18 $Å^{-1}$, which perfectly matches the q-value of the extra-peak in the mixed

mesophase (see Figure 2b). The SAXS profile of dry SPIONs (Figure 2c, red curve) is characterized by an intense peak (centered at 0.07 $Å^{-1}$), which is slightly shifted at higher scattering vectors with respect to the extra-peak in the corresponding mixed mesophase. We attribute the peaks observed for the dry films as arising from interparticle correlations, thereby ascribing the extra-peaks in the hybrid samples to a partial clusterization of NPs along the grain boundaries of the polycrystalline mesophases, as previously shown for similar systems in other studies [13,43,44]. The difference in the correlation length of SPIONs and AuNPs in the dry film might be both related to the core differences or to the slightly different hydrophobic coating of NPs, which might lead to a different arrangement of the alkyl chains between the neighboring NPs.

The shift of the correlation peak from 0.07 $Å^{-1}$ (dry film) to 0.06 $Å^{-1}$ (NPs inside Phyt) observed for SPIONs, which corresponds to a variation in the NP-NP correlation distance from 8.90 to 10.5 nm, hints at the coexistence of SPIONs at the grain boundaries with particles effectively embedded in the mesophase. The same effect is clearer for AuNPs, where an additional correlation peak at 0.097 $Å^{-1}$ is detected, which can unambiguously attributed the appearance of the peak to AuNPs embedded inside the lipid architecture. Interestingly, the estimated correlation distance (6.5 nm) closely matches the nanometric organization of the mesophase.

Upon increasing the NPs amounts, a phase transition from cubic (Pn3m) to hexagonal (H_{II}) phase is detected. In particular, at the lowest NPs amount (light blue lines, Figure 2b, c), both mixed mesophases retain the Pn3m cubic structure; the intermediate amount of SPIONs ($2x10^{-5}$ NPs/Phyt, Figure 2c, green curve) is sufficient to induce the phase transition, while the same number of AuNPs induces a partial transition to the hexagonal phase, highlighted by the coexistence of the typical Bragg reflections of both phases (Figure 2b, green curve); finally, at the highest amount of NPs ($4x10^{-5}$ NPs/Phyt) (Figure 2b, c, yellow curve), both mesophases are H_{II}. In a recent study we reported the same Pn3m-H_{II} phase transition induced by

hydrophobic SPIONs on GMO mesophases, ascribing it to the balance between free energies of elastic curvature and frustration packing [27]. The results here gathered extend our previous findings to a different lipid (Phyt vs GMO), additionally showing that the effect of the hydrophobic nature of SPIONs and AuNPs is similar; even if NPs' number is the same, their different size, results in a difference in volume fractions (See SI for details). This value, higher for SPIONs, fully justifies the less pronounced phase transition of Phyt/AuNPs with respect to the SPIONs mesophase with lower and intermediate amount of NPs. We can conclude that the structural arrangement of the hybrid lipid/hydrophobic NPs mesophases is dependent on: (i) the equilibrium structure of the lipid binary phase; (ii) the hydrophobic nature of the coating of the NPs, leading to their preferential partition in the hydrophobic domains of the lipid scaffold; (iii) the size of NPs, which determines the degree of perturbation of the bilayer curvature at the NPs inclusions, thereby affecting the frustration packing energy of the lipid scaffold [27]. The relevance of this latter parameter is also suggested by the slight variation between SPIONs and AuNPs amounts required to completely trigger the phase transition, fully in line with the slight size and polydispersity difference between the two NPs types.

We then fixed the NPs/Phyt ratio to $1x10^{-5}$ and varied the temperature from 25°C to 50°C, to explore the thermotropic phase behavior of the hybrid mesophases (Figure 3).

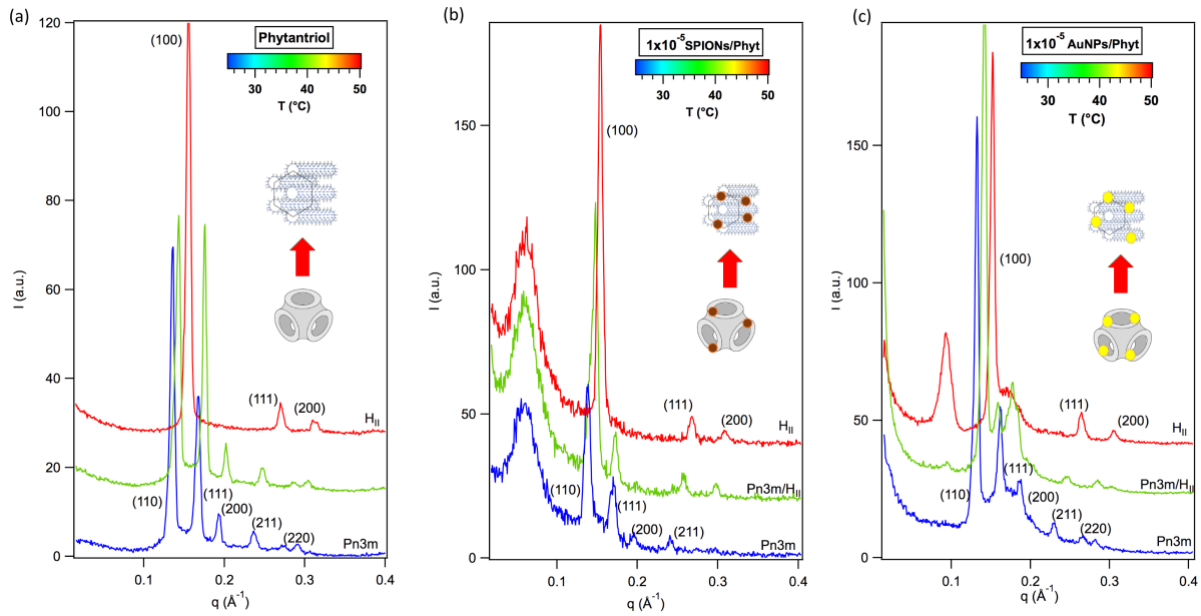

Figure 3. SAXS profiles of Phyt/H_2O mesophases in the absence (a) and in the presence of (b, c) $1x10^{-5}$ NPs ((b) SPIONs and (c) AuNPs) per Phyt molecule at 25 °C (blue), 35 °C (green curves) and 50 °C (red curves); the Miller indexes assignments (hkl) of the Pn3m and hexagonal phase are also reported.

Figure 3a displays the profiles of the binary Phyt/H2O system in excess water, which shows the characteristic Pn3m-H_{II} transition at 50 °C, in full agreement with the literature [40].

Upon loading the same number of SPIONs and AuNPs, (Figures 3b and 3c, respectively) the Pn3m phase persists at room temperature (blue curves); a temperature increase to 35 °C partially promotes the phase transition to the hexagonal phase, both for SPIONs (more pronounced) and for AuNPs (Figure 3b, c green curves). Therefore, the Pn3m-H_{II} transition can be induced both by increasing the amounts of SPIONs and, at a fixed amount of SPIONs, by raising the temperature up to a value which is considerably lower than the transition temperature of binary phase. The correlation peak, observed for higher NPs concentrations (See Figure 2), also appears increasing the temperature with the lower amount of nanoparticles (Figure 3c) and the sharp signal is preserved after 24 h of the thermal cycle (See SI for details). This effect might be related to a reorganization of the NPs which, at higher temperature, are characterized by a higher mobility inside the mesophase. Nevertheless, the present results

further prove that this behavior is not specifically related to a defined lipid molecule or NP kind but can be considered as a general phenomenon. In addition, in this description, the nature of the NPs core does not show major impact.

3.2 Rheological behavior of Phyt mesophases doped with hydrophobic NPs

In order to understand the effect of NPs on the viscoelastic properties of Phyt/NPs systems, rheological experiments were performed on the same hybrid mesophases.

Amplitude sweep measurements at a fixed frequency of 1 Hz and at T=25°C are shown in Figure 4, where the storage modulus G' (the elastic component of the complex modulus G*) and the loss modulus G'' (the dissipative component of G*) of the different liquid crystalline mesophases are displayed as a function of the applied strain. The curves measured for the hybrid Pn3m mesophase doped with $1x10^{-5}$ NPs per Phyt molecule (red markers, SPIONs in Figure 4a, AuNPs in Figure 4c) are compared to those measured for Phyt/H_2O in the absence of NPs (blue markers). Figures 4b, d show the profiles measured for hybrid H_{II} mesophases doped with increasing amounts (light blue markers $2x10^{-5}$ NPs per Phyt molecule, green markers $4x10^{-5}$ NPs per Phyt molecule) of NPs (SPIONs in Figure 4c, AuNPs in Figure 4d).

It is known that different structural arrangements of liquid crystalline mesophases are characterized by markedly diverse rheological responses [43,45]. Accordingly, the inclusion of NPs (both SPIONs and AuNPs) in the Phyt/H_2O cubic mesophase, which induces a cubic-to-hexagonal phase transition, is associated with a striking variation in the rheological behavior: as a matter of fact, for Phyt/H_2O system and for low NPs loading, the amplitude sweep curves (Figures 4a, c) are characterized by the typical behavior of a 3D isotropic network, with no preferential directionality, e.g., similarly to Xantan Gum [46] and PVA [47]-based gels. In particular, G'' shows a non-monotonic behavior: after an initial increase for low strain values, it reaches a maximum, above which a strain increase causes the disruption of the

network, resulting in the decrease of both G' and G", previously interpreted by McLeish and coworkers with a "slip-plane" model, where the local cubic order is disrupted along the direction of applied shear, while the bulk connectivity of the 3D network is preserved [48,49].

As discussed in the previous section, NPs promote the Pn3m to H_{II} phase transition (see Figure 2). The 1D-directional nature of the hexagonal phase, whose domains are able to align along the shear direction [50], determines a very different behavior, with monotonic decrease of both *moduli* with increasing strain (Figures 4b, d).

In summary, the arrangement of the lipid scaffold appears as the main factor affecting the rheological behavior, as inferred from amplitude sweep measurements. Within the same structural arrangement (Pn3m or H_{II}), increasing the NPs number density does not have major effects. This evidence also suggests an overall structural integrity of the mesophase, where lipid assembly persists in the presence of NPs embedded in the hydrophobic domains.

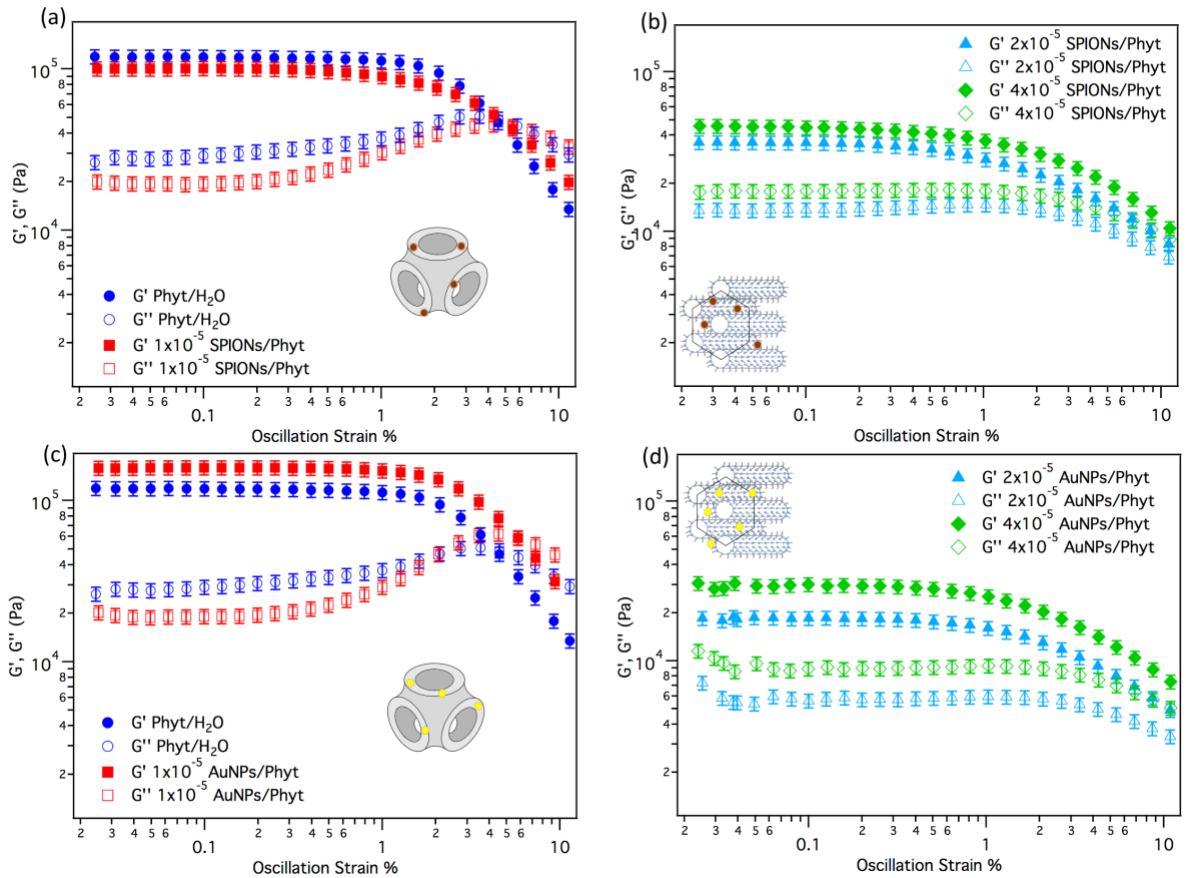

Figure 4. Amplitude sweep analysis performed at 1 Hz and 25 °C for: (a,c) Phyt/H_2O Pn3m mesophase in the absence (blue markers) and in the presence (red markers) of $1x10^{-5}$ SPIONs (a) and AuNPs (c) per Phyt molecule; (b, d) Phyt/H_2O H_{II} mesophase in the presence of $2x10^{-5}$ (light blue markers) and $4x10^{-5}$ (green markers) SPIONs (b) and AuNPs (d) per Phyt molecule.

To gather additional insight into the flow behavior, we investigated the dependence of the storage and loss moduli of the material on the frequency of the applied shear perturbation, by performing frequency sweep measurements in the linear viscoelastic regime (strain 0.1%, see Materials and Methods for details). The main results are reported in Figure 5.

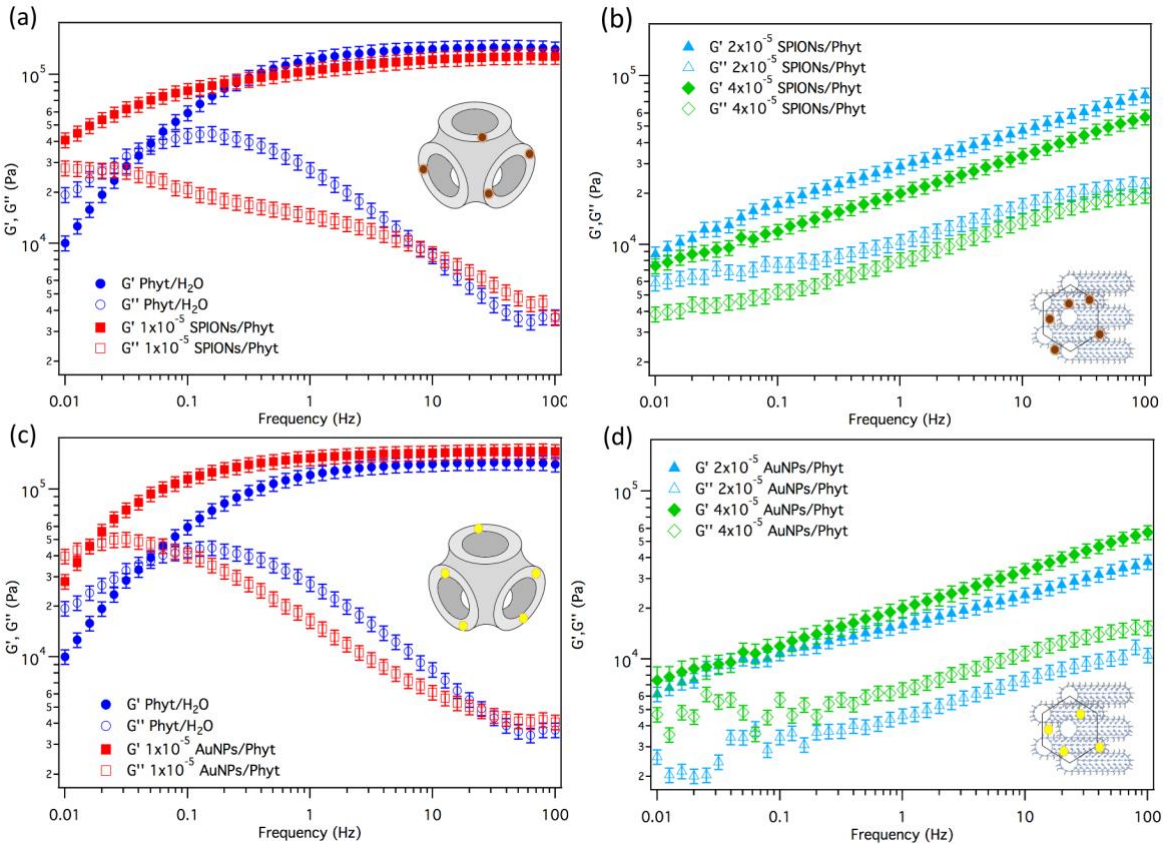

Figure 5. Frequency sweep curves measured at 25°C for: (a,c) Phyt/H_2O Pn3m mesophase in the absence (blue markers) and in the presence (red markers) of $1x10^{-5}$ SPIONs (a) and AuNPs (c) per Phyt molecule; (b, d) Phyt/H_2O H_{II} mesophase in the presence of $2x10^{-5}$ (light blue markers) and $4x10^{-5}$ (green markers) SPIONs (b) and AuNPs (d) per Phyt molecule.

In line with the amplitude sweep profiles, the results highlight a different dependence of both G' and G'' on the frequency of the applied strain for Pn3m (Figures 5a, c) and H_{II} (Figures 5b, d) mesophases. As a first observation, the transition from Pn3m to H_{II} induces a decrease of

G', highlighting the lower rigidity of the hexagonal phase [51,52], which can be again attributed to the transition from a 3D-to-1D geometry, as confirmed by the trend of tanδ (tanδ = G''/G') reported in the SI.

The Pn3m mesophases (Figure 5a, c) behave as a viscoelastic fluid: for $\omega > \omega_c$ (with ω_c crossover frequency between G' and G" curves), G' is higher than G", which indicates a predominantly elastic behavior, while the viscous character is dominant for $\omega < \omega_c$. Concerning the H_{II} mesophase (Figure 5b, d), the material is characterized by a solid-like behavior, with G' higher than G'' in the whole range of investigated frequencies. In this region of the phase diagram, increasing the number density of NPs does not significantly affect the viscoelastic properties, probably due to the alignment of nanoparticles along the hexagonal domains.

Conversely, the inclusion of nanoparticles in a Pn3m mesophase, significantly modifies its rheological behavior. In particular, although the same general trend described for the binary phase is preserved for the cubic phases doped with SPIONs (Figure 5a, red markers) and AuNPs (Figure 5c, red markers), the crossover frequency between G' and G'' is shifted to lower ω values. This effect is particularly marked for SPIONs, with the crossover frequency located outside the accessible frequency range of our rheometer.

The crossover frequency marks the transition from the rubbery plateau to the viscous regime and corresponds to the longest relaxation time ($\tau_{max} = 1/\omega_c$) of the system, i.e. the longest characteristic time required to relax back to the equilibrium configuration. According to the model proposed by Mezzenga et al. [45,53], the physical meaning of this relaxation time $\tau_{max} = 1/\omega_c$ can be attributed to the diffusion time of the lipid molecules at the water-lipid interface; this value provides therefore a characteristic order of magnitude for the diffusion processes occurring at the interface and can be used as an indication for the release kinetics of the active molecule through the hydrophobic/hydrophilic interface [53]. The τ_{max} value markedly increases in the presence of $1x10^{-5}$ NPs/Phyt, passing from 3.1 s to 10 s for AuNPs

and to > 10 s for SPIONs, accounting for a slower response of the material to the applied stress, which is a clear signature of an enhanced solid-like behavior.

To rule out that this effect is caused by the partition of the SPIONs coating agents in the bilayer (added also to Phyt/AuNPs, to better compare the two systems, see SI for details), we performed a control experiment where the same amount of oleic acid and oleylamine was directly added to Phyt without NPs (See SI for details). This results in a negligible shift in the crossover frequency with respect to the neat binary phase. Therefore, the possible compositional change of the lipid scaffold determined by these hydrophobic molecular additives, does not substantially affect the lipid/water interface relaxation time.

Moreover, as discussed in the SAXS section, the NPs affect the lattice parameter of the mesostructure, shrinking the water channels. Since it has been reported [52] that the swelling of the cubic phase has a major impact on the crossover frequency values, as a further control experiment we performed rheological experiments on Phyt/oleic acid/oleylamine Pn3m mesophases, tuning the composition to match the lattice parameter of NPs/Phyt (see SI). The variation of the frequency sweep profile is indeed negligible and therefore possible effects due to a different degree of swelling of the cubic phase can be safely ruled out.

In summary, the presence of NPs is the main factor that tunes the viscoelastic relaxation of the cubic mesophase. To better appreciate this point, the frequency sweep curves were transformed in continuum relaxation spectra [45,52] (Figure 6, see SI for the different inversion methods tested). The behavior of Pn3m cubic mesophases can be described with a monomodal distribution of relaxation times: the main term is identified with the characteristic diffusion time of lipids at the water-lipid interface, i.e. τ_{max}.

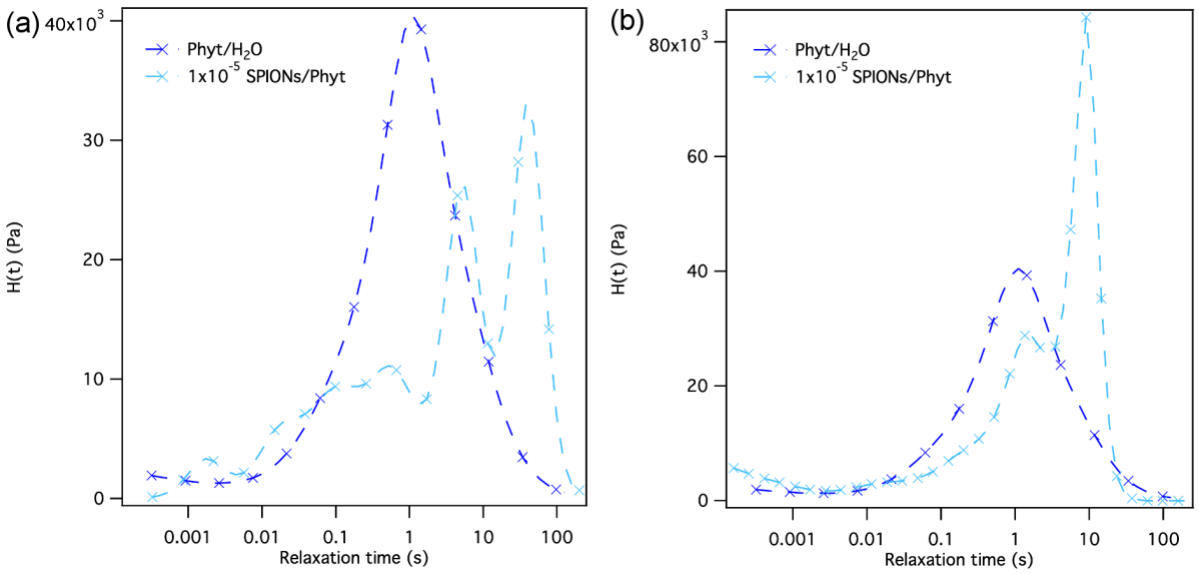

Figure 6: Viscoelastic relaxation spectra of Pn3m mesophases: Phyt/H_2O (blue markers and line in both plots), Phyt/SPIONs (cyan markers and line in (a)), and Phyt/AuNPs (cyan markers and line in (b)).

With NPs, the relaxation mode distribution broadens and the spectrum complexity increases, indicating higher polidispersity [52]. For both kinds of NPs, the main relaxation mode splits into a multimodal distribution, suggesting a non-trivial effect on the rheological properties of lipid bilayer. This feature can be interpreted in terms of the coexistence of lipids freely diffusing at the lipid/water interface, with a slower relaxation time, i.e. τ_{max}, ascribable to a hampered lipid diffusion at the NPs' surface.

Interestingly, this is a similar effect highlighted through Fluorescence Correlation Spectroscopy [54,55], for hydrophilic AuNPs interacting with free-standing lipid membrane.

Moreover, although the NPs' diameter is comparable, the concentration identical and the effects on phase behavior similar (as highlighted from SAXS measurements), the addition of SPIONs is related to a significantly higher τ_{max} value with respect to AuNPs (9.1 s vs 37.9 s), as the comparison between Figure 6a and b, highlights. Therefore, the chemical nature of NPs might be critical for the rheological response of the material. This significant effect is, we believe, well beyond what can be expected considering the slight difference in NPs sizes,

therefore hinting to a "core" effect in the viscoelastic response. A working hypothesis is that the long-range dipolar interaction between the SPIONs, which are absent in the AuNPs-doped systems, act as a structuring factor on the material, increasing the elastic over viscous response of the material upon the applied stress. This stiffening effect likely originates at the nanoscale level, where dipolar interactions between SPIONS inside the bilayer may additionally hamper the free diffusion of lipids. Indeed, while AuNPs do not significantly influence the diffusion times of lipid molecules at the lipid/water interface, corresponding to the higher- τ peak in the relaxation spectrum (Figure 6b, light blue dashed line), SPIONs cause a substantial shift in the "free-diffusion" time of lipids, suggesting an alteration of molecular mobility in the whole bilayer.

4. CONCLUSIONS

In this contribution we explored the structural and rheological effects of the insertion of hydrophobic SPIONs and AuNPs of similar size in liquid crystalline mesophases of Phytantriol at maximum water swelling. SAXS results highlighted that both types of NPs are embedded in the liquid crystalline mesophase and that their presence promotes a cubic to hexagonal phase transition, with no noteworthy dependence on the type of NPs, but only on their number density, in line with previous data on glycerol-monooleate/SPIONs hybrid mesophases [27]. These results are consistent with the fact that simple thermodynamic considerations, related to the mesophase geometry, the coating and size of NP, can describe in general terms the phase behavior.

The rheological response of such architectures, addressed here for the first time, reveals that the presence of NPs enhances the solid-like behavior of the material. Interestingly, this effect is significantly more pronounced for SPIONs, evidencing possible long-range dipolar

interactions between SPIONs that may constitute an additional structuring factor for the material, decreasing its deformability upon stress deformation.

Overall, the comparison of structural and rheological results highlights that different features of the NPs are relevant in affecting the properties of the mesophase: NPs surface (i.e., hydrophobic nature of the coating, driving localization in the lipid scaffold) and size, modulate the local perturbation of the lipid assemblies and affect the phase behavior at rest, while the core composition (AuNPs vs SPIONs) seem to become relevant for the rheological response and for the relaxation to mechanical perturbation.

These results shed light on the structural and physicochemical properties of lipid/NPs mixed liquid crystalline mesophases, disclosing new fundamental knowledge for future biomedical applications.

ACKNOWLEDGMENT

Mirko Severi is gratefully acknowledged for ICP-AES analysis; CSGI is acknowledged by all the authors for partial funding.

ASSOCIATED CONTENT

Supplementary Materials and Methods, Supplementary SAXS and rheology data.

REFERENCES

[1] W.K. Fong, T.L. Hanley, B. Thierry, A. Tilley, N. Kirby, L.J. Waddington, B.J. Boyd, Understanding the photothermal heating effect in non-lamellar liquid crystalline systems, and the design of new mixed lipid systems for photothermal on-demand drug delivery, Phys. Chem. Chem. Phys. 16 (2014) 24936–24953. doi:10.1039/c4cp03635b.

[2] W.K. Fong, T.L. Hanley, B. Thierry, N. Kirby, B.J. Boyd, Plasmonic nanorods provide reversible control over nanostructure of self-assembled drug delivery materials, Langmuir. 26 (2010) 6136–6139. doi:10.1021/la100644s.

[3] I.L. Medintz, H.T. Uyeda, E.R. Goldman, H. Mattoussi, Quantum dot bioconjugates for

imaging, labelling and sensing, Nat. Mater. 4 (2005) 435–446. doi:10.1038/nmat1390.

[4] J.A. Kloepfer, N. Cohen, J.L. Nadeau, FRET between CdSe quantum dots in lipid vesicles and water- And lipid-soluble dyes, J. Phys. Chem. B. 108 (2004) 17042–17049. doi:10.1021/jp048094c.

[5] G. Gopalakrishnan, C. Danelon, P. Izewska, M. Prummer, P.Y. Bolinger, I. Geissbühler, D. Demurtas, J. Dubochet, H. Vogel, Multifunctional lipid/quantum dot hybrid nanocontainers for controlled targeting of live cells, Angew. Chemie - Int. Ed. 45 (2006) 5478–5483. doi:10.1002/anie.200600545.

[6] W.T. Al-jamal, K.T. Al-jamal, B. Tian, L. Lacerda, P.H. Bomans, P.M. Frederik, K. Kostarelos, Lipid Quantum Dot Bilayer Vesicles, ACS Nano. 2 (2008).

[7] K. Yang, Y. Liu, Y. Liu, Q. Zhang, C. Kong, C. Yi, Z. Zhou, Z. Wang, G. Zhang, Y. Zhang, N.M. Khashab, X. Chen, Z. Nie, Cooperative Assembly of Magneto-Nanovesicles with Tunable Wall Thickness and Permeability for MRI-Guided Drug Delivery, (2018). doi:10.1021/jacs.8b00884.

[8] M.S. Martina, J.P. Fortin, C. Ménager, O. Clément, G. Barratt, C. Grabielle-Madelmont, F. Gazeau, V. Cabuil, S. Lesieur, Generation of superparamagnetic liposomes revealed as highly efficient MRI contrast agents for in vivo imaging, J. Am. Chem. Soc. 127 (2005) 10676–10685. doi:10.1021/ja0516460.

[9] E. Amstad, J. Kohlbrecher, E. Müller, T. Schweizer, M. Textor, E. Reimhult, Triggered release from liposomes through magnetic actuation of iron oxide nanoparticle containing membranes, Nano Lett. 11 (2011) 1664–1670. doi:10.1021/nl2001499.

[10] A. Salvatore, C. Montis, D. Berti, P. Baglioni, Multifunctional Magnetoliposomes for Sequential Controlled Release, ACS Nano. 10 (2016) 7749–7760. doi:10.1021/acsnano.6b03194.

[11] C.C. Piccinetti, C. Montis, M. Bonini, R. Laurà, M.C. Guerrera, G. Radaelli, F. Vianello, V. Santinelli, F. Maradonna, V. Nozzi, A. Miccoli, I. Olivotto, Transfer of Silica-Coated Magnetic (Fe 3 O 4) Nanoparticles Through Food: A Molecular and Morphological Study in Zebrafish, Zebrafish. 11 (2014) 567–579. doi:10.1089/zeb.2014.1037.

[12] M. Szlezak, D. Nieciecka, A. Joniec, M. Pękała, E. Gorecka, M. Emo, M.J. Stébé, P. Krysiński, R. Bilewicz, Monoolein Cubic Phase Gels and Cubosomes Doped with Magnetic Nanoparticles–Hybrid Materials for Controlled Drug Release, ACS Appl. Mater. Interfaces. (2017) acsami.6b12889. doi:10.1021/acsami.6b12889.

[13] E. Venugopal, S.K. Bhat, J.J. Vallooran, R. Mezzenga, Phase behavior of lipid-based lyotropic liquid crystals in presence of colloidal nanoparticles, Langmuir. 27 (2011) 9792–9800. doi:10.1021/la201767p.

[14] C. Fong, T. Le, C.J. Drummond, Lyotropic liquid crystal engineering–ordered nanostructured small molecule amphiphile self-assembly materials by design, Chem. Soc. Rev. 41 (2012) 1297. doi:10.1039/c1cs15148g.

[15] N. Tran, A.M. Hawley, J. Zhai, B.W. Muir, C. Fong, C.J. Drummond, X. Mulet, High-Throughput Screening of Saturated Fatty Acid Influence on Nanostructure of Lyotropic Liquid Crystalline Lipid Nanoparticles., Langmuir. 32 (2016) 4509–20. doi:10.1021/acs.langmuir.5b03769.

[16] N. Tran, X. Mulet, A.M. Hawley, C. Fong, J. Zhai, T.C. Le, J. Ratcliffe, C.J. Drummond, Manipulating the Ordered Nanostructure of Self-Assembled Monoolein and Phytantriol Nanoparticles with Unsaturated Fatty Acids, Langmuir. 34 (2018) 2764–2773. doi:10.1021/acs.langmuir.7b03541.

[17] S. Aleandri, C. Speziale, R. Mezzenga, E.M. Landau, Design of Light-Triggered Lyotropic Liquid Crystal Mesophases and Their Application as Molecular Switches in 'On Demand' Release, Langmuir. 31 (2015) 6981–6987. doi:10.1021/acs.langmuir.5b01945.

[18] K.J. Tangso, W.K. Fong, T. Darwish, N. Kirby, B.J. Boyd, T.L. Hanley, Novel spiropyran amphiphiles and their application as light-responsive liquid crystalline components, J. Phys. Chem. B. 117 (2013) 10203–10210. doi:10.1021/jp403840m.

[19] S. Jia, J.D. Du, A. Hawley, W.K. Fong, B. Graham, B.J. Boyd, Investigation of Donor-Acceptor Stenhouse Adducts as New Visible Wavelength-Responsive Switching Elements for Lipid-Based Liquid Crystalline Systems, Langmuir. 33 (2017) 2215–2221. doi:10.1021/acs.langmuir.6b03726.

[20] Q. Liu, Y. Da Dong, B.J. Boyd, Selective Sequence for the Peptide-Triggered Phase Transition of Lyotropic Liquid-Crystalline Structures, Langmuir. 32 (2016) 5155–5161. doi:10.1021/acs.langmuir.6b00547.

[21] L. Van'T Hag, L. De Campo, C.J. Garvey, G.C. Feast, A.E. Leung, N.R. Yepuri, R. Knott, T.L. Greaves, N. Tran, S.L. Gras, C.J. Drummond, C.E. Conn, Using SANS with Contrast-Matched Lipid Bicontinuous Cubic Phases to Determine the Location of Encapsulated Peptides, Proteins, and Other Biomolecules, J. Phys. Chem. Lett. 7 (2016) 2862–2866. doi:10.1021/acs.jpclett.6b01173.

[22] L. van 't Hag, A. Anandan, S.A. Seabrook, S.L. Gras, C.J. Drummond, A. Vrielink, C.E. Conn, Direct demonstration of lipid phosphorylation in the lipid bilayer of the biomimetic bicontinuous cubic phase using the confined enzyme lipid A phosphoethanolamine transferase, Soft Matter. 13 (2017) 1493–1504. doi:10.1039/C6SM02487D.

[23] J.M. Bulpett, T. Snow, B. Quignon, C.M. Beddoes, T.-Y.D. Tang, S. Mann, O. Shebanova, C.L. Pizzey, N.J. Terrill, S.A. Davis, W.H. Briscoe, Hydrophobic nanoparticles promote lamellar to inverted hexagonal transition in phospholipid mesophases., Soft Matter. 11 (2015) 8789–800. doi:10.1039/c5sm01705j.

[24] C.M. Beddoes, J. Berge, J.E. Bartenstein, K. Lange, A.J. Smith, R.K. Heenan, W.H. Briscoe, Hydrophilic nanoparticles stabilising mesophase curvature at low concentration but disrupting mesophase order at higher concentrations, Soft Matter. 12 (2016) 6049–6057. doi:10.1039/C6SM00393A.

[25] J.J. Vallooran, R. Negrini, R. Mezzenga, Controlling anisotropic drug diffusion in lipid-Fe3O4 nanoparticle hybrid mesophases by magnetic alignment, Langmuir. 29 (2013) 999–1004. doi:10.1021/la304563r.

[26] J.J. Vallooran, S. Bolisetty, R. Mezzenga, Macroscopic alignment of lyotropic liquid crystals using magnetic nanoparticles, Adv. Mater. 23 (2011) 3932–3937. doi:10.1002/adma.201101760.

[27] M. Mendozza, C. Montis, L. Caselli, M. Wolf, P. Baglioni, D. Berti, On the thermotropic and magnetotropic phase behavior of lipid liquid crystals containing magnetic

nanoparticles, Nanoscale. 10 (2018) 3480–3488. doi:10.1039/c7nr08478a.

[28] C. Montis, B. Castroflorio, M. Mendozza, A. Salvatore, D. Berti, P. Baglioni, Magnetocubosomes for the delivery and controlled release of therapeutics, J. Colloid Interface Sci. 449 (2015) 317–326. doi:10.1016/j.jcis.2014.11.056.

[29] L. Boge, A. Västberg, A. Umerska, H. Bysell, J. Eriksson, K. Edwards, A. Millqvist-Fureby, M. Andersson, Freeze-dried and re-hydrated liquid crystalline nanoparticles stabilized with disaccharides for drug-delivery of the plectasin derivative AP114 antimicrobial peptide, J. Colloid Interface Sci. 522 (2018) 126–135. doi:10.1016/j.jcis.2018.03.062.

[30] U. Bazylińska, J. Kulbacka, J. Schmidt, Y. Talmon, S. Murgia, Polymer-free cubosomes for simultaneous bioimaging and photodynamic action of photosensitizers in melanoma skin cancer cells, J. Colloid Interface Sci. 522 (2018) 163–173. doi:10.1016/j.jcis.2018.03.063.

[31] N. Tran, M. Hocquet, B. Eon, P. Sangwan, J. Ratcliffe, T.M. Hinton, J. White, B. Ozcelik, N.P. Reynolds, B.W. Muir, Non-lamellar lyotropic liquid crystalline nanoparticles enhance the antibacterial effects of rifampicin against Staphylococcus aureus, J. Colloid Interface Sci. 519 (2018) 107–118. doi:10.1016/j.jcis.2018.02.048.

[32] Q. Liu, J. Hu, M.R. Whittaker, T.P. Davis, B.J. Boyd, Nitric oxide-sensing actuators for modulating structure in lipid-based liquid crystalline drug delivery systems, J. Colloid Interface Sci. 508 (2017) 517–524. doi:10.1016/j.jcis.2017.08.079.

[33] M. Raudino, G. Selvolini, C. Montis, M. Baglioni, M. Bonini, D. Berti, P. Baglioni, Polymer films removed from solid surfaces by nanostructured fluids: Microscopic mechanism and implications for the conservation of cultural heritage, ACS Appl. Mater. Interfaces. 7 (2015). doi:10.1021/acsami.5b00534.

[34] M. Mamusa, L. Sitia, F. Barbero, A. Ruyra, T.D. Calvo, C. Montis, A. Gonzalez-Paredes, G.N. Wheeler, C.J. Morris, M. McArthur, D. Berti, Cationic liposomal vectors incorporating a bolaamphiphile for oligonucleotide antimicrobials, Biochim. Biophys. Acta - Biomembr. 1859 (2017). doi:10.1016/j.bbamem.2017.06.006.

[35] M. Brust, M. Walker, D. Bethell, D.J. Schiffrin, R. Whyman, Synthesis of thiol-

derivatised gold nanoparticles in a two-phase liquid-liquid system, J. Chem. Soc. Chem. Commun. (1994) 801–802. doi:10.1039/C39940000801.

[36] M. Kotlarchyk, S.-H. Chen, Analysis of small angle neutron scattering spectra from polydisperse interacting colloids, J. Chem. Phys. 79 (1983) 2461. doi:10.1063/1.446055.

[37] L. Wang, J. Luo, Q. Fan, M. Suzuki, I.S. Suzuki, M.H. Engelhard, Y. Lin, N. Kim, J.Q. Wang, C.J. Zhong, Monodispersed core-shell Fe 3O 4@Au nanoparticles, J. Phys. Chem. B. 109 (2005) 21593–21601. doi:10.1021/jp0543429.

[38] H. Sub Wi, K. Lee, H. Kyu Pak, Interfacial energy consideration in the organization of a quantum dot–lipid mixed system, J. Phys. Condens. Matter. 20 (2008) 494211. doi:10.1088/0953-8984/20/49/494211.

[39] J. Barauskas, T. Landh, Phase behavior of the phytantriol/water system, Langmuir. 19 (2003) 9562–9565. doi:10.1021/la0350812.

[40] J. Barauskas, T. Landh, Phase Behavior of the Phytantriol/Water System, Langmuir. 19 (2003) 9562–9565. doi:10.1021/la0350812.

[41] J. Xie, C. Xu, N. Kohler, Y. Hou, S. Sun, Controlled PEGylation of Monodisperse Fe3O4 Nanoparticles for Reduced Non-Specific Uptake by Macrophage Cells, Adv. Mater. 19 (2007) 3163–3166. doi:10.1002/adma.200701975.

[42] J. Chen, M.A. Reed, C.L. Asplund, A.M. Cassell, M.L. Myrick, A.M. Rawlett, J.M. Tour, P.G. Van Patten, Placement of conjugated oligomers in an alkanethiol matrix by scanned probe microscope lithography, Appl. Phys. Lett. 75 (1999) 624–626. doi:10.1063/1.124461.

[43] J.B. Marlow, M.J. Pottage, T.M. McCoy, L. De Campo, A. Sokolova, T.D.M. Bell, R.F. Tabor, Structural and rheological changes of lamellar liquid crystals as a result of compositional changes and added silica nanoparticles, Phys. Chem. Chem. Phys. 20 (2018) 16592–16603. doi:10.1039/C8CP02101E.

[44] J.J. Vallooran, S. Handschin, S. Bolisetty, R. Mezzenga, Twofold light and magnetic responsive behavior in nanoparticle-lyotropic liquid crystal systems, Langmuir. 28 (2012) 5589–5595. doi:10.1021/la300449q.

[45] R. Mezzenga, C. Meyer, C. Servais, A.I. Romoscanu, L. Sagalowicz, R.C. Hayward, Shear rheology of lyotropic liquid crystals: A case study, Langmuir. 21 (2005) 3322–3333. doi:10.1021/la046964b.

[46] K. Hyun, M. Wilhelm, C.O. Klein, K.S. Cho, J.G. Nam, K.H. Ahn, S.J. Lee, R.H. Ewoldt, G.H. McKinley, A review of nonlinear oscillatory shear tests: Analysis and application of large amplitude oscillatory shear (LAOS), Prog. Polym. Sci. 36 (2011) 1697–1753. doi:10.1016/j.progpolymsci.2011.02.002.

[47] K. Hyun, S.H. Kim, K.H. Ahn, S.J. Lee, Large amplitude oscillatory shear as a way to classify the complex fluids, J. Nonnewton. Fluid Mech. 107 (2002) 51–65. doi:Pii S0377-0257(02)00141-6\rDoi 10.1016/S0377-0257(02)00141-6.

[48] S. Radiman, C. Toprakcioglu, T. McLeish, Rheological Study of Ternary Cubic Phases, Langmuir. 10 (1994) 61–67. doi:10.1021/la00013a009.

[49] J.L. Jones, T.C.B. McLeish, Rheological Response of Surfactant Cubic Phases, Langmuir. 11 (1995) 785–792. doi:10.1021/la00003a020.

[50] G. Schmidt, P. Lindner, I. Laue-langevin, Small-angle neutron scattering from a hexagonal phase under shear, Colloid Polym. Sci. 88 (1996) 85–88. doi:10.1007/BF00658914.

[51] M. Pouzot, R. Mezzenga, M. Leser, L. Sagalowicz, S. Guillote, O. Glatter, Structural and rheological investigation of Fd3m inverse micellar cubic phases, Langmuir. 23 (2007) 9618–9628. doi:10.1021/la701206a.

[52] C. Speziale, R. Ghanbari, Rheology of Ultraswollen Bicontinuous Lipidic Cubic Phases, (2018). doi:10.1021/acs.langmuir.8b00737.

[53] L. Sagalowicz, R. Mezzenga, M.E. Leser, Investigating reversed liquid crystalline mesophases, 11 (2006) 224–229. doi:10.1016/j.cocis.2006.07.002.

[54] C. Montis, A. Zendrini, F. Valle, S. Busatto, L. Paolini, A. Radeghieri, A. Salvatore, D. Berti, P. Bergese, Size distribution of extracellular vesicles by optical correlation techniques, Colloids Surfaces B Biointerfaces. 158 (2017). doi:10.1016/j.colsurfb.2017.06.047.

[55] C. Montis, D. Maiolo, I. Alessandri, P. Bergese, D. Berti, Interaction of nanoparticles with lipid membranes: a multiscale perspective, Nanoscale. 6 (2014) 6452–6457. doi:10.1039/C4NR00838C.